Joule

CellPress

Article

Full Spectrum Solar Thermal Energy Harvesting and Storage by a Molecular and Phase-Change Hybrid Material

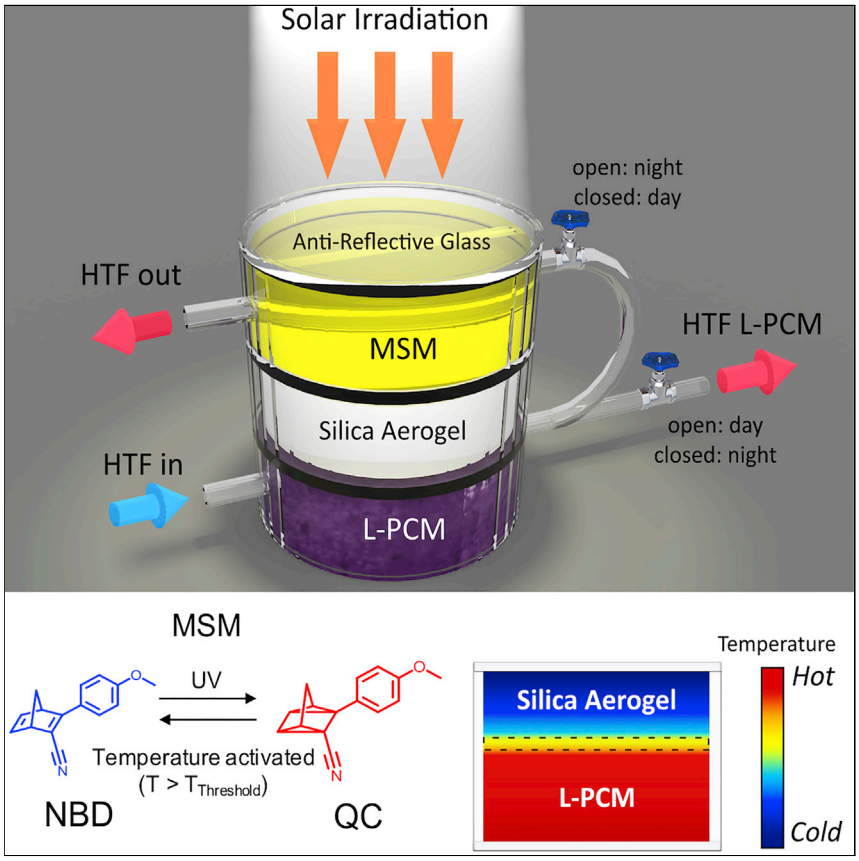

An integrated hybrid system for simultaneous harvesting and storage of solar thermal energy.

Varun Kashyap, Siwakorn Sakunkaewkasem, Parham Jafari, ..., Maria D. Marquez, T. Randall Lee, Hadi Ghasemi

trlee@uh.edu (T.R.L.)
hghasemi@uh.edu (H.G.)

HIGHLIGHTS

Hybrid system combines the concepts of molecular energy and latent heat storage

Energy release both during day and night time operations

Stored energy recovery at night with higher temperature than during the day

Integrated system with simultaneous harvesting and storage of solar thermal energy

Kashyap et al., Joule 3, 3100–3111
December 18, 2019
https://doi.org/10.1016/j.joule.2019.11.001

Joule

CellPress

Article

Full Spectrum Solar Thermal Energy Harvesting and Storage by a Molecular and Phase-Change Hybrid Material

Varun Kashyap,[1] Siwakorn Sakunkaewkasem,[2] Parham Jafari,[1] Masoumeh Nazari,[1] Bahareh Eslami,[1] Sina Nazifi,[1] Peyman Irajizad,[1] Maria D. Marquez,[2] T. Randall Lee,[2,*] and Hadi Ghasemi[1,3,*]

SUMMARY

Efficient solar thermal energy harvesting and storage are critical steps toward utilizing the abundant solar irradiation that reaches the surface of the earth. Current solar thermal approaches rely on costly high optical concentration systems, leading to high heat losses by hot bulk materials and surfaces. At the same time, the energy stored in the form of thermal energy has inherently large temporal losses. Here, we combine the physics of molecular energy and latent heat storage to introduce an integrated, simultaneous harvesting and storage hybrid paradigm for potential 24/7 energy delivery. The hybrid paradigm utilizes heat localization during the day to provide a harvesting efficiency of 73% at small scale and ~90% at large scale. Remarkably, at night, the stored energy by the hybrid system is recovered with an efficiency of 80% and at a higher temperature than that of the day, in contrast to all of the state-of-the-art systems.

INTRODUCTION

Among the many renewable energy sources available, solar energy is gaining increasing importance because of the promising potential it holds to satisfy human energy needs.[1–5] The amount of energy utilized by humans annually, which is approximately 4.6×10^{20} joules, is provided by the sun in merely 1 h. Three main approaches are employed for solar energy conversion, solar electric approaches (i.e., photovoltaics), solar thermal energy approaches[6–8] (e.g., power generation), and solar water splitting (H_2 production).[9] Although the sun provides ~0.12 MW of power to the earth, solar electricity only accounts for ~0.015% of the global energy need, while this value is 0.3% for solar thermal technologies. This void in efficient utilization of solar energy justifies a need for disruptive technologies to harvest and store thermal energy from the sun.

Most current technologies utilize separate infrastructures for harvesting and storing energy. A heat transfer fluid (HTF) must circulate between both infrastructures to store energy.[10] This leads to large thermal losses due to long piping lines and high costs associated with complex systems including heat exchangers that are required in these systems.[11] The figures of merit for solar thermal energy harvesting are efficiency and operating temperature, while for storage technologies, the metrics are energy density (MJ/m^3), specific energy (MJ/kg), and operating temperature.[12] These storage media can be broadly classified into two groups: thermophysical storage (i.e., sensible heat storage and latent heat storage[13,14]) and thermochemical storage. Thermophysical energy-storage media are thermally stable at high operating temperatures but suffer from low energy densities.

Context & Scale

The physics of molecular energy and phase-change storage is combined to introduce a hybrid paradigm for potential 24/7 energy delivery using solar thermal energy. An integrated system is developed for simultaneous harvesting and storage of energy. In large-scale operations, this integrated system helps mitigate thermal losses that exist in conventional systems because of long piping lines and high costs associated with complex systems including heat exchangers. In this system, energy is released both during the day and night operations. Furthermore, at night, stored energy is recovered at 80% efficiency and at a higher temperature than during the day, which is an inherent advantage to other state-of-the-art systems. This general concept can be used with any combination of molecular storage and phase-change materials to build optimal systems for specific applications including power generation and desalination.

Thermochemical storage technologies utilize endothermic and exothermic chemical reactions to store solar thermal energy.[15] Although these latter systems have high energy densities, their drawbacks include weak long-term durability, low chemical stability, and complicated reactors for specific chemical reactions.

In another method called "molecular energy storage," a parent photoswitchable molecule absorbs sunlight and undergoes photoisomerization to a high-energy state.[16] The isomerization process, in which one molecule changes into a different molecule while maintaining the same atomic composition, stores energy within the bonds of the molecule as enthalpy. The absorbed energy can then be released either by using a catalyst or with heat to isomerize back to the parent molecule. This approach is attractive since the chemical energy can be stored in a compact way without requiring thermal insulation.[17] Several photoisomers have been identified and used for molecular energy storage, including anthracene,[18] difulvalenediruthenium complexes,[19] dihydroazulene and vinylheptafulvene,[20] Dewar isomers of azaborinine derivatives,[21] azobenzene,[16,22–24] and norbornadiene-quadricyclane (NBD-QC) derivatives.[25–28] Among the aforementioned photoisomers, the NBD-QC system has proven to be a promising material because of its high specific energy (0.4 MJ/kg), long storage times ($t_{1/2}$ = 30 days at 25°C), and exceptional heat release.[28] Isomerization in the NBD-QC system in previous reports was triggered using a UV light source and a catalyst (e.g., cobalt phthalocyanine on a carbon support) was used to trigger the back-isomerization (QC-NBD) reaction for energy release under vacuum conditions. However, no solar energy harvesting and release has been demonstrated for these materials.

Herein, we report the concept of a molecular and phase-change hybrid that combines the concepts of molecular energy storage and latent heat storage to capture the full solar spectrum for long-term operation, both during the day and night cycles. Performance of both individual layers of the hybrid system and the entire hybrid system have been studied elaborately in this work. The physics of heat localization[29–32] is employed in this hybrid material to obtain the required phase-change temperature at low solar concentrations. During the day, the heat from the localized phase-change material (L-PCM) is harvested by the HTF with ~73% efficiency, at small scale, while the molecular storage material (MSM) captures the UV radiation from the solar spectrum, shown in Figure 1A. At night, heat from both the L-PCM and MSM is harvested by the HTF with ~80% efficiency. Furthermore, the energy required for the thermal back isomerization of the MSM material is provided by the L-PCM.

Molecular and Phase-Change Hybrid Model

We introduce a general hybrid concept composed of a MSM and L-PCM to achieve full spectrum solar energy harvesting and storage to provide thermal energy both during the day and night, as shown in Figure 1A. During the day, the L-PCM, the bottom layer, absorbs the incident solar irradiation and undergoes a solid-liquid phase transition. The concept of solar heat localization[33–38] is employed to reach the phase-transition temperature at low solar flux and minimize heat loss. Carbonized rayon (CR), which has high absorption (>97%) in the solar spectrum, is introduced in the phase-change material (PCM) to localize the heat and create a hot spot in the material structure. To minimize radiation losses from the top surface of the L-PCM, the L-PCM is covered with a bulk silica aerogel layer, which is transparent in the solar spectrum and opaque in the infrared spectrum.[39] Furthermore, the silica aerogel allows for a constant temperature difference to exist between the L-PCM and MSM, a critical component for daytime functionality of the hybrid system. The

[1]Department of Mechanical Engineering, University of Houston, 4726 Calhoun Road, Houston, TX 77204-4006, USA

[2]Department of Chemistry and the Texas Center for Superconductivity, University of Houston, Houston, TX 77204-5003, USA

[3]Lead Contact

*Correspondence: trlee@uh.edu (T.R.L.), hghasemi@uh.edu (H.G.)

https://doi.org/10.1016/j.joule.2019.11.001

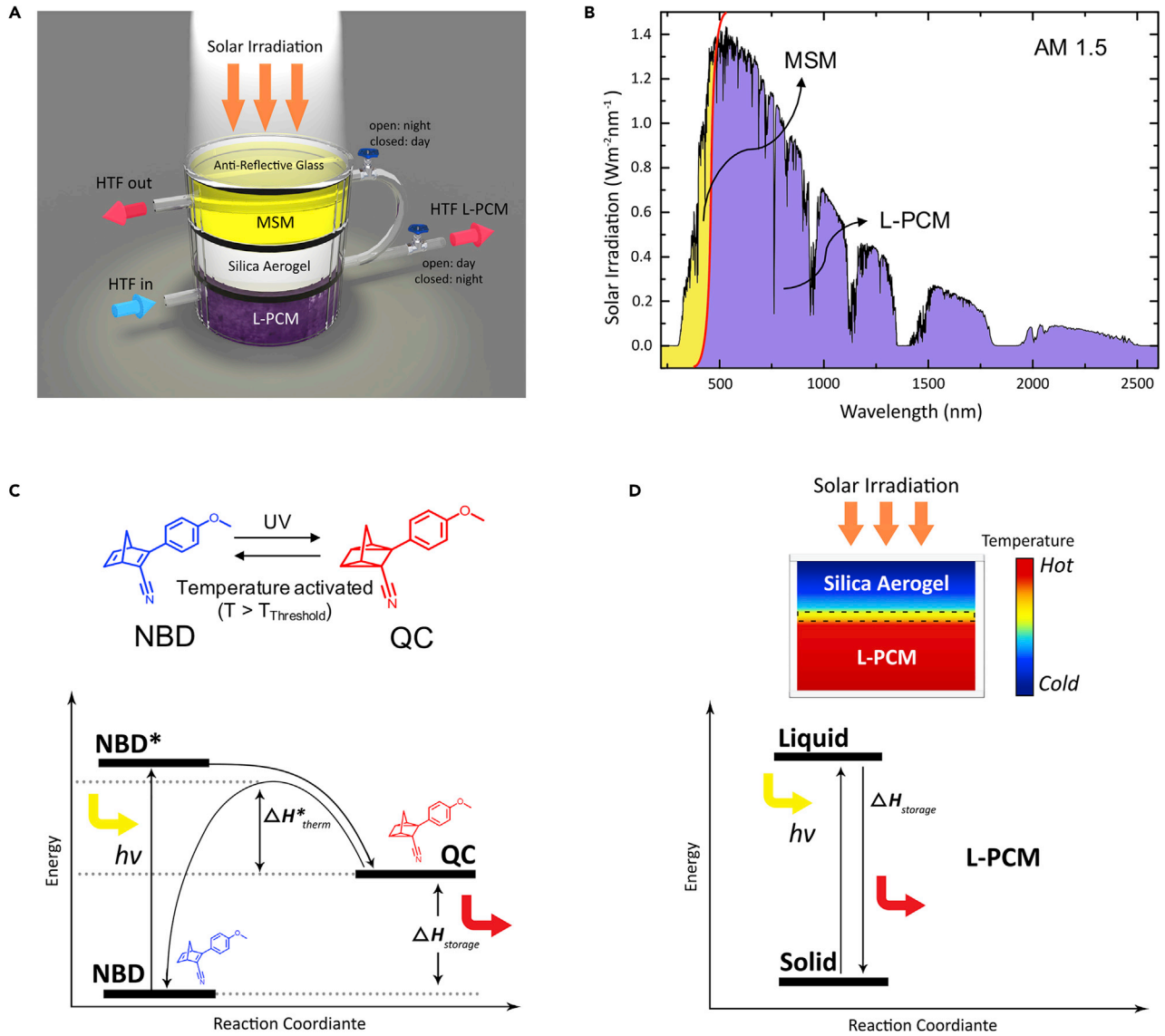

Figure 1. Concept of Full Spectrum Solar Thermal Energy Harvesting and Storage

(A) Illustration of the molecular and phase-change hybrid. The hybrid consists of a molecular storage material (MSM) and a localized phase-change material (L-PCM) separated by a silica aerogel to maintain the necessary temperature difference.

(B) Wavelengths of the solar spectrum captured by the MSM and L-PCM are shown.

(C) The concept of molecular energy storage is illustrated. The norbornadiene (NBD) derivative undergoes photoisomerization to the corresponding quadricyclane (QC) derivative upon exposure to UV radiation and undergoes back isomerization upon thermal initiation.

(D) The concept of phase-change energy storage is shown. Energy is stored in the form of enthalpy.

dimensional design of the aerogel layer and its role on heat transfer is discussed in a later section. Heat is stored in the L-PCM in the form of latent heat. A HTF is circulated through the L-PCM to harvest the stored energy. On the other side, the MSM is composed of a photoisomer. During the day, the photoisomer absorbs UV radiation to induce isomerization of the MSM while at the same time storing energy. Important to note is the low temperature (<70°C) needed during the harvesting of UV radiation by the photoisomer to maximize efficiency. During the night, the HTF from the L-PCM, which is at the phase-transition temperature, flows to the MSM to provide the necessary threshold temperature to initiate the thermal back

isomerization; this process releases the energy stored from the UV radiation. Thus, the hybrid system absorbs the complete solar spectrum and provides thermal energy both during the day and night (potentially 24/7). A salient feature of this hybrid system is the higher harvesting temperature at night, compared to daytime temperatures, which is an inherent advantage to state-of-the-art systems.[13,25]

Figure 1B shows wavelengths of the solar spectrum harvested by the MSM and L-PCM layers. In a sample model of this general concept, we used a combination of 54.1% KNO_3, 20% $NaNO_3$, and 25.9% $LiNO_3$ as the PCM[40,41] and the norbornadiene (NBD)-quadricyclane (QC)[28] system shown in Figure 1C as the MSM material. We selected a combination of KNO_3, $NaNO_3$, and $LiNO_3$ because of its high energy density and low melting point (~120°C),[41] which can be achieved under low solar flux. Details of the synthesis of the MSM are provided in the Supplemental Information. We chose the NBD-QC system because of its high specific energy (0.4 MJ/kg).[28] Note that this combination of PCM and MSM was used to illustrate the concept of a molecular and phase-change hybrid system. However, the system presented herein is not limited to the aforementioned combination; in fact, any combination of PCM and MSM can be used in this hybrid system. The ultraviolet-visible (UV-vis) absorption spectrum for the PCM is shown in Figure S1. CR, which is introduced within the PCM, absorbs the incoming solar radiation, converts it to heat, and supplies this heat to the PCM to initiate the phase change. Although an absorption peak is seen for the PCM in the UV range of the solar spectrum (λ = 300 nm), Figure S1, the use of the MSM is critical in harvesting UV radiation effectively. The MSM releases absorbed energy during the back-isomerization process at night and provides significantly higher output temperatures (T_{out}) without compromising the efficiency of the system.

Figure 1C also shows the reaction energy diagram for photoisomerization of the NBD-QC system. The parent NBD derivative undergoes isomerization to the high-energy QC derivative upon exposure to UV photons. Conversely, the QC derivative, upon thermal initiation, isomerizes back to the parent molecule and releases the absorbed energy. Energy storage in the L-PCM occurs through a solid-liquid phase change and is illustrated in Figure 1D; the temperature gradient in the L-PCM and silica aerogel layer is also shown for reference. Specifically, the L-PCM localizes incident solar irradiation generating a hot spot, while the silica aerogel preserves the required low temperature (<70°C) on the surface. This strategy ensures that the MSM is always below the threshold temperature to harvest UV radiation during the day without initiating back isomerization. Furthermore, as shown in Figure 1D, the change in enthalpy attributed to the phase change is released as energy during the phase transition of the L-PCM from liquid to solid.

RESULTS AND DISCUSSION

Full Spectrum Solar Energy Harvesting during the Day

The daytime performance of the hybrid system toward harvesting energy is shown in Figure 2; the experimental setup is shown in Figure S2. The HTF enters the system at ambient temperature (T_{in}). The output temperature from the L-PCM, T_{out} (L-PCM), is a function of the Reynolds number (Re) of flow of the HTF. Figure 2A shows T_{out} (L-PCM) as a function of solar irradiation and the Re. T_{out} (L-PCM) increases as the Re decreases and solar irradiation increases. Figure 2B shows the thermal efficiency of the L-PCM as a function of the Re and is given by

$$\eta = \frac{\dot{m} C_p \Delta T}{\tau Q_{in}} \qquad \text{(Equation 1)}$$

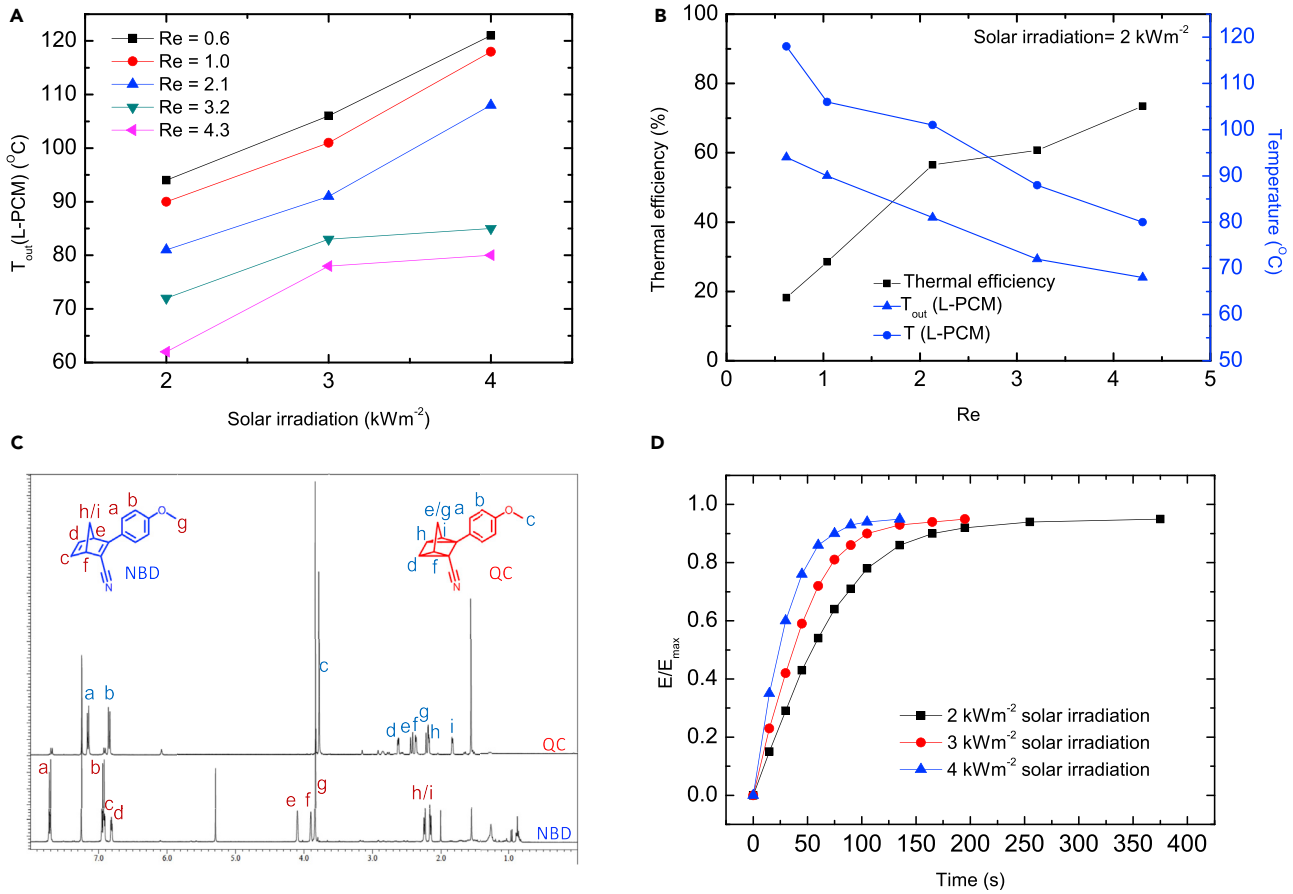

Figure 2. Solar Thermal Energy Harvesting during the Day

(A) T_{out} (L-PCM) as a function of solar concentration and Reynolds number for HTF flow is shown.

(B) Thermal efficiency for solar thermal energy harvesting during the day is shown as a function of the surface temperature of the PCM and Reynolds number for HTF flow.

(C) The proton NMR spectra showing complete conversion of the NBD isomer to the QC isomer under UV radiation is shown.

(D) Transient change in energy stored by the MSM during photoisomerization of the NBD derivative to the QC derivative under varying solar concentrations is shown.

where $\dot{m}$ is the mass flow rate of the HTF in kgs^{-1}, C_p is the specific heat of the HTF used (silicone oil) in $Jkg^{-1}\,K^{-1}$, ΔT is the temperature difference between T_{in} and T_{out} (L-PCM) in K, τ is the transmission across 3 glasses (including one anti-reflective glass and the silica aerogel monolith), and $\dot{Q}_{in}$ is the illuminated solar irradiation in W. As shown in Figure 2B, thermal efficiency increases as a function of the Re for a fixed solar irradiation. For other solar irradiations, the relationships are shown in Figures S3 and S4. For 2 kWm^{-2} solar irradiation, a maximum thermal efficiency of ~73% is obtained during the day for a small-scale system.

To confirm isomerization of the NBD derivative to the QC derivative in the presence of UV light (300–370 nm) in solution, ^{1}H NMR spectroscopy was performed before and after irradiation (see Figure 2C). The MSM was dispersed in toluene since the photoisomer exhibits good ambient stability in toluene ($t_{1/2}$ = 30 days at 25°C).[28] The conversion occurs through the photosensitized cyclization of the NBD moiety via [2 + 2] intramolecular cyclization. To confirm the existence of the NBD and QC species, separately, both compounds were characterized with ^{1}H NMR spectroscopy. The peaks unique to the NBD isomer, originating from the double bond, at δ ~6.92 (labeled

c in Figure 2C) and δ ~6.82 (labeled d in Figure 2C) disappear from the NMR spectrum after irradiation of the sample and conversion to the QC isomer. This result was observed for both molecules in the hybrid system and for those tested outside the system, which indicates that almost all (≥95%) of the NBD isomer is converted to the QC isomer, and the UV radiation in the solar spectrum is successfully harvested by the MSM, the top layer of the hybrid system. The transient change in stored energy stored by the MSM is shown in Figure 2D and was measured by conversion of the NBD-QC system using UV-vis spectroscopy. Note, the time for the NBD derivative to isomerize to the QC derivative is shorter at high solar irradiations compared to low solar irradiation. For example, at a solar irradiation of 4 kWm^{-2}, complete isomerization to the QC derivative was observed in ~125 s for the MSM at a concentration of 5×10^{-5} M; it is about ~200 s at 3 kWm^{-2} and ~375 s at 2kWm^{-2}.

Solar Energy Storage by Molecular Phase-Change Hybrid

The solar thermal energy-storage capabilities of the individual MSM and L-PCM along with the molecular phase-change hybrid system are evaluated in Figure 3. Differential scanning calorimetry (DSC) was conducted on the QC derivative, as shown in Figure 3A. Samples of the QC isomer were prepared by exposing the toluene solution of the NBD isomer to 365 nm UV light. The volatile toluene solution was evaporated, and complete conversion was confirmed by ^{1}H NMR spectroscopy prior to conducting the DSC measurements, as shown in Figures S5A and S5B. DSC was conducted for two continuous heating cycles, from 40°C to 180°C. During the first heating cycle (continuous line in Figure 3A), heat release is observed at ~85°C. The experimental energy storage is shown to be $\Delta H_{storage}$ = 88 kJ mol^{-1}, corresponding to an energy density of 0.4 MJ kg^{-1}. However, during the second heating cycle, no heat release was observed (dashed line in Figure 3A), thereby indicating the complete conversion of the QC isomer to the NBD isomer during the first heating cycle. The phase-change diagram and DSC for the PCM is provided in the Supplemental Information (Figures S6 and S7).

The storage capacities of our system and those of state-of-the-art energy-storage materials are compared in Figure 3B. The energy density versus specific energy diagram is considered as the figure of merit for assessment of energy-storage materials.[12] As discussed by Gur et al.,[12] the ideal energy-storage material should have both high energy density and specific energy. Furthermore, the phase-change temperatures of various materials are also provided in Figure 3B. To illustrate the applicability of the proposed concept of a hybrid molecular and phase-change system, a PCM with a phase-transition temperature of ~120°C was used. This temperature was targeted because of the appeal of low solar concentration and the associated reduced operation costs in comparison to high concentration systems. Note that any PCM can be used in this system employing the same concept. The energy-storage metrics of both the MSM and the L-PCM used in this study are given in Figure 3B. As shown, the specific energy of the molecular and phase-change hybrid is higher than L-PCM by using a coupled MSM system, thereby proving higher storage capacities of the hybrid system.

The interchangeable formation of the NBD and QC isomers is illustrated in Figures 3C and 3D. The key structural difference between the NBD and QC isomers is the extended conjugation present in the NBD isomer, which includes the aromatic ring, the double bond in the norbornadiene ring, and the nitrile group. This small conjugated system significantly shifts the highest absorbance peak to a lower absorption wavelength compared to the QC isomer. In a smaller conjugated system, more energy is required to excite the π electron in the electronic transition (higher highest occupied molecular orbital [HOMO]-lowest unoccupied molecular orbital [LUMO] gaps)

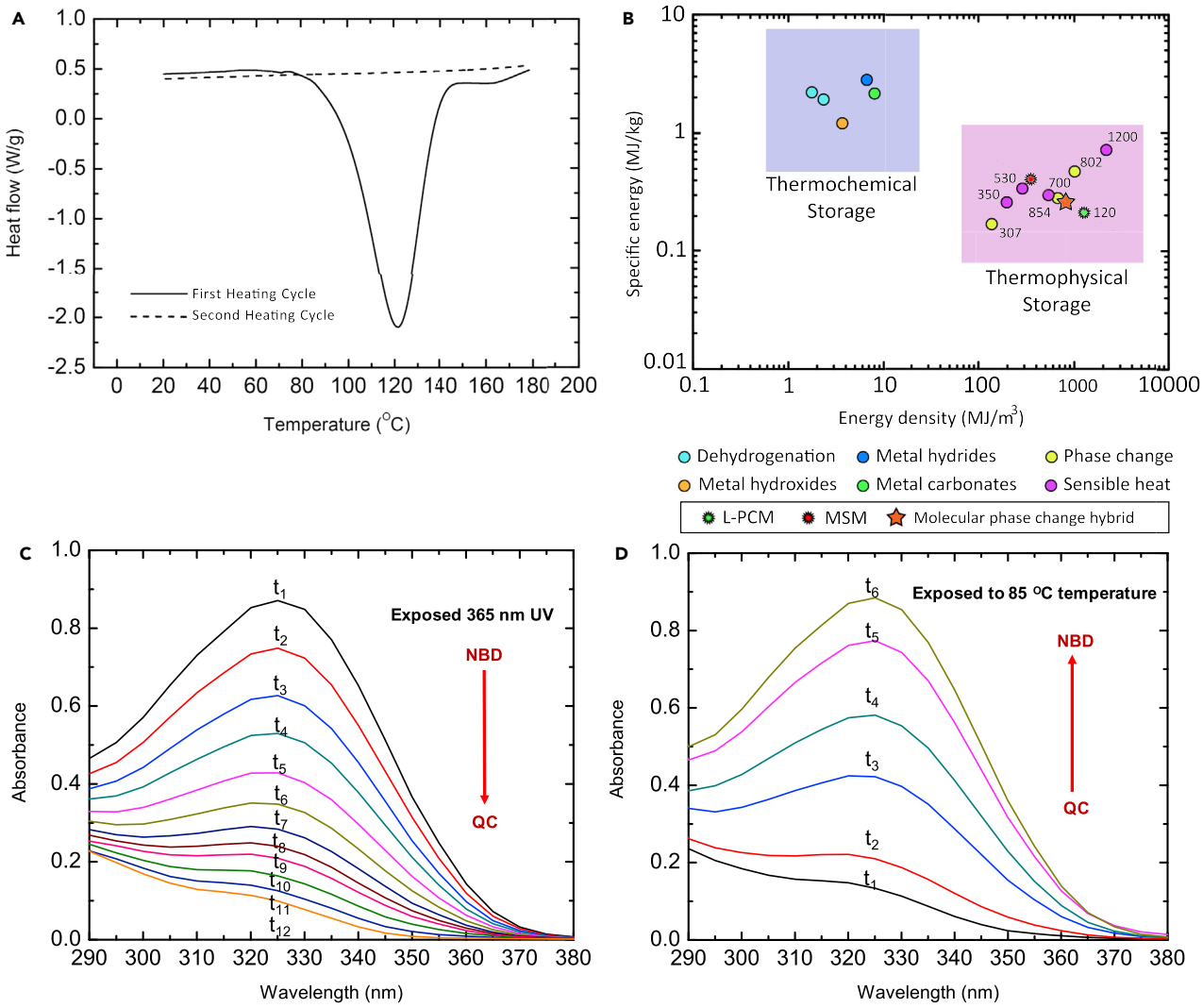

Figure 3. Solar Thermal Energy Storage by Molecular Phase-Change Hybrid

(A) DSC thermogram is shown for the thermal back conversion of the QC derivative to the NBD derivative. The solid line represents the first heating cycle and the dashed line represents the second heating cycle.

(B) Storage capacities of state-of-the-art energy-storage materials are compared, including thermochemical and thermophysical storage mechanisms. It is seen that harvesting the full spectrum of the incident solar irradiation increases the specific energy.

(C and D) UV-vis spectra illustrating the forward photoisomerization process (C) and thermal back isomerization process (D) are shown.

compared to a larger conjugation system. Thus, after exposure to a UV source, 365 nm for 30 s, a decrease in the intensity of the peak at 325 nm was observed. Upon increasing UV irradiation time on the NBD-containing solution, a linearly decreasing trend was observed. This process was repeated until the absence of the absorption peak at ~325 nm was noted. The disappearance of the peak at ~325 nm ensures the complete transformation of the NBD isomer to the QC isomer. To reobtain the NBD isomer, the reverse chemical transformation was performed by applying heat to the QC-containing solution. As discussed earlier, the QC derivative is reversed back to the NBD derivative by thermal initiation. The conversion proceeds through a retro-[2 + 2] intramolecular cyclization. Upon exposing the QC-containing solution to an ~85°C oil bath, the absorption peak at ~325 nm begins to increase in intensity, indicating formation of the extended conjugation system. This experiment was

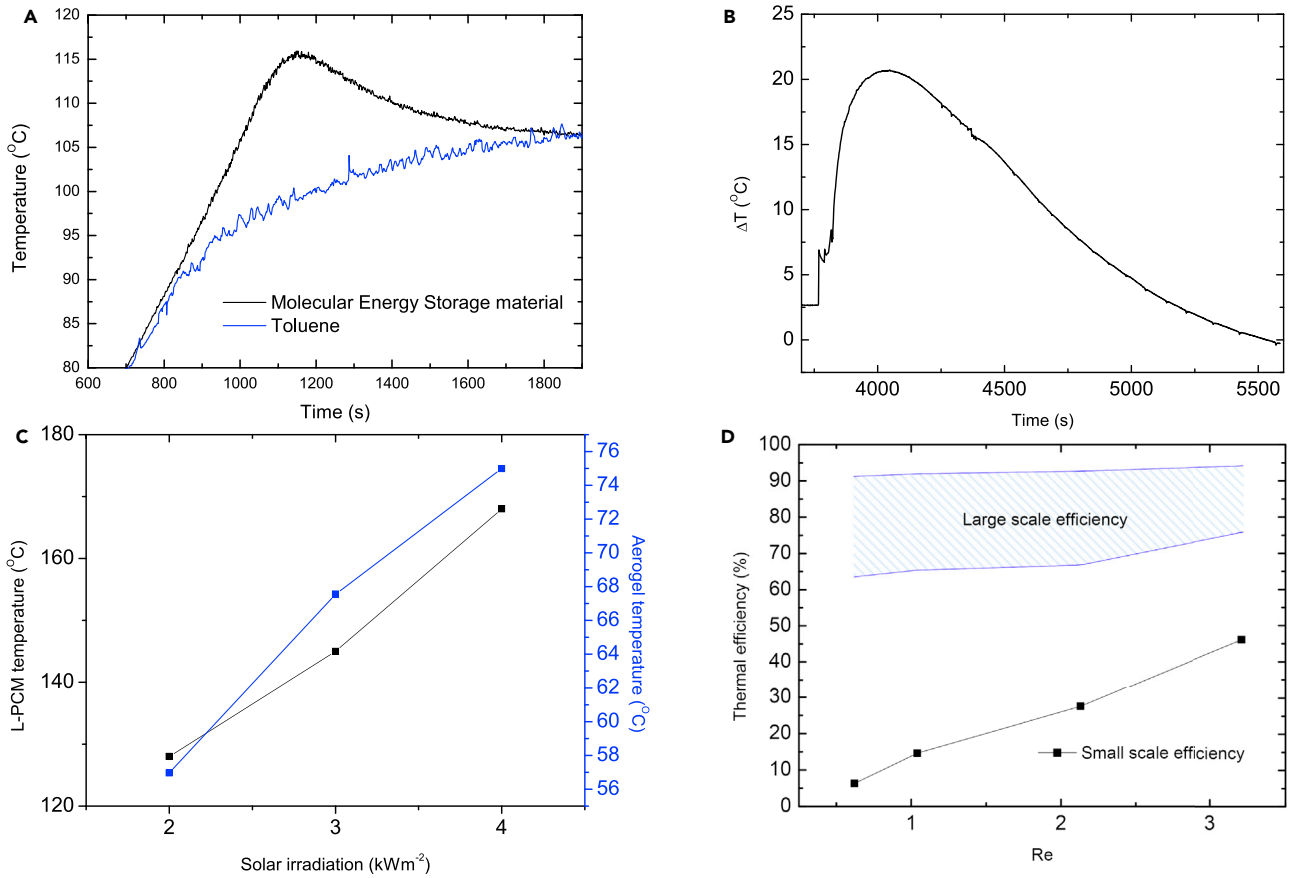

Figure 4. Full Spectrum Solar Energy Harvesting during Night

(A) Transient heat release of toluene and the MSM (QC derivative) dispersed in toluene are compared. As shown, a clear temperature jump is seen in the case of toluene.

(B) The transient temperature difference between the HTF outlet from the L-PCM and the outlet from the MSM for a Reynolds number of 1.0 is shown. A clear peak that is associated with the heat release is seen.

(C) The steady-state temperature of the L-PCM and the temperature of the glass above the aerogel are shown as a function of solar irradiation. The average aerogel temperature is ~70°C for an average L-PCM temperature of ~140°C.

(D) Both small- and large-scale thermal efficiencies of energy harvested by the MSM are plotted as a function of Reynolds number. A range of large-scale efficiencies are shown based on the thickness of the insulating layer used to cover the top surface. This large-scale efficiency can reach as high as ~94%.

continued until no further change in the absorbance was noted. The absorbance data before exhibiting photosensitized cyclization and after retro-[2 + 2] intramolecular cyclization exhibited similar values, as shown in Figure 3C.

Energy Harvesting during the Night

During nighttime operation (no solar irradiation), energy is harvested both from the L-PCM and MSM. During the daytime, the L-PCM attains high steady-state temperatures of up to ~170°C and T_{out} (L-PCM) of >100°C. This temperature is higher than the $T_{threshold}$ for activation of the MSM for energy release. Once the HTF flows through the MSM, it harvests the energy stored in it. To confirm energy release by the MSM, both the MSM (as the QC isomer) and pure toluene were heated to the threshold temperature simultaneously. As shown in Figure 4A, the MSM showed a temperature jump of 10°C to 15°C, as opposed to pure toluene, which exhibited a constant temperature increase. These results are consistent with the heat release shown in Figure 3A. This property of the MSM is exploited in the hybrid system to achieve a high final outlet HTF temperature. The temperature difference between

the outlet from the L-PCM (T_{out} (L-PCM)) and the outlet from the MSM (T_{out}) is shown in Figure 4B and corresponds to a Re of 1.0. The latent heat release from the L-PCM heats the HTF and elevates its temperature beyond the threshold temperature for the thermal back isomerization of the MSM (QC), which is >85°C.

As mentioned earlier, in order for the NBD derivative to completely undergo photo-isomerization to the QC derivative, the temperature of the MSM must be maintained at a temperature below the threshold temperature. Figure 4C shows that the average temperature on top of the aerogel glass is ~70°C, for an average L-PCM temperature of ~145°C (which is above the phase-change temperature of the L-PCM). Therefore, the hybrid system can be operated up to a solar irradiation of 4 kWm^{-2} while maintaining an MSM temperature below the threshold temperature for thermal back isomerization. Figure 4D shows the thermal efficiency of the MSM as a function of Re. The thermal efficiency of the MSM is given by

$$\eta_{thermal} = \frac{\dot{m}C_p \int_0^t (T_{out} - T_{out}(L-PCM))\, dt}{\Delta E_{storage\ MSM}}. \qquad \text{(Equation 2)}$$

Where $\Delta E_{storage\ MSM}$ is the total energy that is stored by the MSM by molecular energy storage and sensible heat in joules. Note that the term $\int_0^t (T_{out} - T_{out}(L-PCM))\, dt$ is obtained from Figure 4B for different Res. A maximum efficiency of ~47% was obtained for the MSM at a high flow rate (Re = 3.2) while achieving a maximum T_{out} of ~119°C. The two-dimensional (2D) side losses associated with a small-scale experiment were simulated and are presented in Figure S8. These losses can be avoided for large-scale experiments, thereby increasing the efficiency further up to 76%. This efficiency can be further increased as a function of the thickness of the insulating layer used on the top surface for nighttime operation. Both large- and small-scale thermal efficiencies of the MSM are shown in Figure 4D as a function of Re. The breakdown of the losses is elaborated in the Supplemental Information (Table S1).

Performance of the Molecular and Phase-Change Hybrid System

Figure 5 shows the performance of the complete molecular and phase-change hybrid system for both daytime and nighttime operations. The thermal efficiency of the aerogel monolith on top of the L-PCM is obtained from the Rosseland diffusion approximation.[39] Based on this approximation, the temperature field is determined and the corresponding aerogel thermal efficiency is calculated (Figure 5A). The thickness of the aerogel monolith was calculated based on optimal aerogel efficiency. The aerogel efficiency is shown as a function of L-PCM surface temperature in Figure 5A. At low L-PCM surface temperatures, aerogel efficiency is as high as 90%. Small-scale efficiency for daytime operation of the hybrid system for 2 sun solar irradiation is shown in Figure 5B. The efficiency formulation is explained in an earlier section. Based on the aerogel efficiency from Figure 5A, the surface and 2D losses are calculated. Note that for large-scale operation, the 2D losses are negligible, and the system efficiency can be increased up to 90%, as shown in Figure 5B. The graphs for solar irradiations of 3 and 4 kWm^{-2} are shown in the Supplemental Information (Figures S9 and S10). Nighttime efficiency of the hybrid system is given by

$$\eta_{hybrid\ system\ (night)} = \frac{\dot{m}C_p \int_o^t (T_{out} - T_{in})dt}{\Delta E_{storage\ L-PCM} + \Delta E_{storage\ MSM} + \Delta E_{storage\ SM}}. \qquad \text{(Equation 3)}$$

Where $\Delta E_{storage\ L-PCM}$ is the total energy stored by the L-PCM—including latent heat and sensible heat—in joules, $\Delta E_{storage\ MSM}$ is the total energy stored by the MSM by

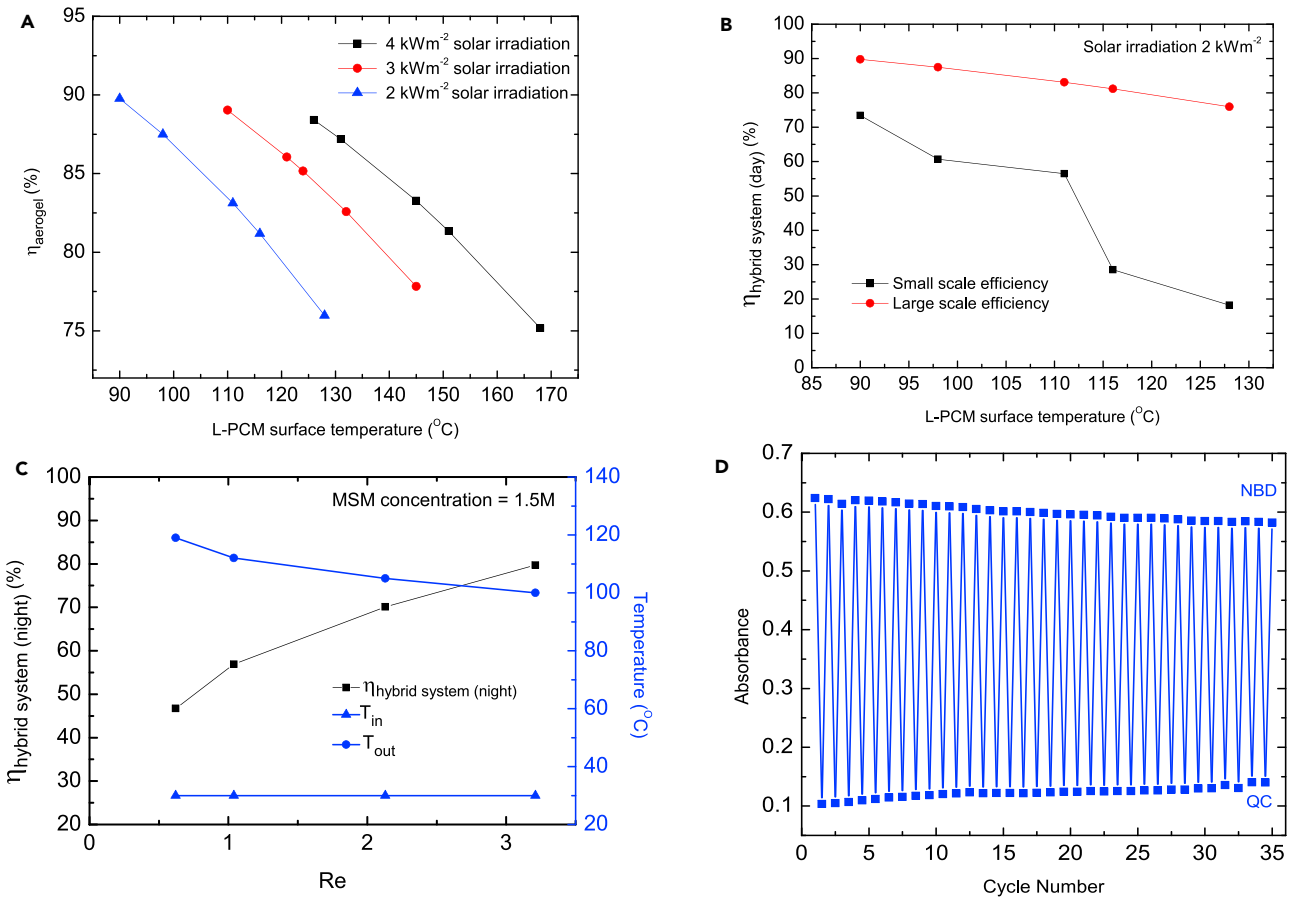

Figure 5. Performance of the Molecular and Phase-Change Hybrid System

(A) The aerogel efficiency is shown as a function of L-PCM surface temperature. The aerogel has a high thermal efficiency of ~ 90% at low solar concentrations.

(B) The efficiency of the hybrid system is shown for daytime energy harvesting as a function of L-PCM surface temperature for small- and large-scale operation. A high thermal efficiency of ~90% was observed for large-scale operation.

(C) The nighttime efficiency of the hybrid system and the final output temperature of the HTF are shown as a function of Reynolds number. The system exhibits a nighttime efficiency of ~80% while providing the HTF at an output temperature of ~119°C.

(D) The cyclic performance of the MSM is evaluated in isomerization and thermal back-isomerization reactions for 35 cycles. Degradation of the MSM over 35 cycles was negligible (0.2%).

molecular energy storage and sensible heat in joules, and $\Delta E_{storage\ SM}$ represents the component of the input heat that is stored in the surrounding media as sensible heat in joules. Note that the term $\int_o^t (T_{out} - T_{in})dt$ is obtained from Figure S11 for different Res. The energy balance for the system and the energies stored by both the L-PCM and MSM are described in detail in the Supplemental Information (Section 13). The calculations for surface losses are also explained in the Supplemental Information (Table S2). The hybrid system offers ~80% efficiency while delivering the HTF at an output temperature of ~119°C during nighttime operation. This opens up a wide array of applications where the solar energy can be stored during the day and harvested during the night at high temperatures, including water heating, power generation, and sterilization. Cyclic experiments were conducted to evaluate the stability of the MSM over several operating cycles. The NBD isomer was converted to the QC isomer under UV illumination, and complete conversion was verified using UV-vis spectroscopy. Thermal back isomerization was initiated on a

heating stage at 85°C, and complete back conversion was again confirmed by UV-vis spectroscopy. This process was carried out for 35 cycles, and a negligible degradation of 0.2% was seen over 35 cycles as shown in Figure 5D.

Conclusions

We developed a hybrid concept where we coupled the physics of molecular energy storage by photoisomerization and phase-change energy storage by latent heat to harvest thermal energy from the sun and provide a potential 24/7 energy supply. The hybrid system absorbs the complete solar spectrum with minimal degradation of material, even after 35 cycles of operation. We achieved a high hybrid system efficiency of 73% for energy harvesting during the day, at 2 kWm^{-2} solar irradiation, which can be increased to ~90% for large-scale operation and an efficiency of ~80% for energy harvesting during the night. Note that this concept can be used for different combinations of PCM and MSM materials to achieve higher energy densities. This new paradigm opens up various avenues for harvesting solar thermal energy at high efficiency and low operation cost for a wide spectrum of applications, including desalination, power generation, and distillation.

SUPPLEMENTAL INFORMATION

Supplemental Information can be found online at https://doi.org/10.1016/j.joule.2019.11.001.

ACKNOWLEDGMENTS

The authors gratefully acknowledge funding support from the Air Force Office of Scientific Research (grant AFOSR FA9550-16-1-0248, H.G.) with Dr. Ali Sayir as program manager, the Robert A. Welch Foundation (E-1320, T.R.L.), and the Texas Center for Superconductivity (T.R.L.). They also thank Andrew Eisterhold and Dr. Ognjen Miljanic from the Department of Chemistry, University of Houston for help with microwave experiments.

AUTHOR CONTRIBUTIONS

H.G., T.R.L., V.K., and S.S. conceived the idea. V.K. and S.S. conducted the experiments. P.J., S.N., and P.I. helped in the design and development of the experimental setups. B.E. and M.N. helped in analyzing the data. M.D.M. helped with chemical synthesis and analysis. V.K., S.S., T.R.L., and H.G. wrote the manuscript, and all authors commented on the manuscript. T.R.L. and H.G. directed the research.

DECLARATION OF INTERESTS

The authors declare no competing interests.

Received: August 16, 2019
Revised: September 22, 2019
Accepted: October 31, 2019
Published: November 20, 2019

REFERENCES

1. Lewis, N.S. (2010). Solar energy use. Science *798*, 80.
2. Lewis, N.S. (2016). Research opportunities to advance solar energy utilization. Science *351*, aad1920.
3. Sadeghpour, A., Zeng, Z., Ji, H., Ebrahimi, N.D., Bertozzi, A.L., and Ju, Y.S. (2019). Water vapor capturing using an array of traveling liquid beads for desalination and water treatment. Sci. Adv. *5*, 1–9.
4. Zeng, Z., Sadeghpour, A., and Ju, Y.S. (2019). A highly effective multi-string humidifier with a low gas stream pressure drop for desalination. Desalination *449*, 92–100.
5. Chu, S., and Majumdar, A. (2012). Opportunities and challenges for a sustainable energy future. Nature *488*, 294–303.
6. Zalba, B., Marín, J.M., Cabeza, L.F., and Mehling, H. (2003). Review on thermal energy storage with phase change: materials, heat transfer analysis and applications. Appl. Therm. Eng. *23*, 251–283.

7. Badenhorst, H. (2018). A review of the application of carbon materials in solar thermal energy storage. Sol. Energy, 35–68.

8. Liu, M., Steven Tay, N.H., Bell, S., Belusko, M., Jacob, R., Will, G., Saman, W., and Bruno, F. (2016). Review on concentrating solar power plants and new developments in high temperature thermal energy storage technologies. Renew. Sustain. Energy Rev. *53*, 1411–1432.

9. Tachibana, Y., Vayssieres, L., and Durrant, J.R. (2012). Artificial photosynthesis for solar water-splitting. Nat. Photonics *6*, 511–518.

10. Cartlidge, E., Nevada, S., Goswami, Y., Florida, S., and Fabrizi, F. (2011). Saving for a rainy day. Science *334*, 922–924.

11. Medrano, M., Gil, A., Martorell, I., Potau, X., and Cabeza, L.F. (2010). State of the art on high-temperature thermal energy storage for power generation. part 2 Case studies. Renew. Sustain. Energy Rev. *14*, 56–72.

12. Gur, I., Sawyer, K., and Prasher, R. (2012). Thermal battery design. Science *64802*, 1454–1455.

13. Kuravi, S., Trahan, J., Goswami, D.Y., Rahman, M.M., and Stefanakos, E.K. (2013). Thermal energy storage technologies and systems for concentrating solar power plants. Prog. Energy Combust. Sci. *39*, 285–319.

14. Kenisarin, M., and Mahkamov, K. (2007). Solar energy storage using phase change materials☆. Renew. Sustain. Energy Rev. *11*, 1913–1965.

15. Pardo, P., Deydier, A., Anxionnaz-Minvielle, Z., Rougé, S., Cabassud, M., and Cognet, P. (2014). A review on high temperature thermochemical heat energy storage. Renew. Sustain. Energy Rev. *32*, 591–610.

16. Kolpak, A.M., and Grossman, J.C. (2011). Azobenzene-functionalized carbon nanotubes as high-energy density solar thermal fuels. Nano Lett. *11*, 3156–3162.

17. Schrader, T.E., Schreier, W.J., Cordes, T., Koller, F.O., Babitzki, G., Denschlag, R., Renner, C., Löweneck, M., Dong, S.L., Moroder, L., et al. (2007). Light-triggered beta-hairpin folding and unfolding. Proc. Natl. Acad. Sci. USA *104*, 15729–15734.

18. Islangulov, R.R., and Castellano, F.N. (2006). Photochemical upconversion: anthracene dimerization sensitized to visible light by a RuII chromophore. Angew. Chem. Int. Ed. Engl. *45*, 5957–5959.

19. Moth-Poulsen, K., Ćoso, D., Börjesson, K., Vinokurov, N., Meier, S.K., Majumdar, A., Vollhardt, K.P.C., and Segalman, R.A. (2012). Molecular solar thermal (MOST) energy storage and release system. Energy Environ. Sci. *5*, 8534–8537.

20. Vlasceanu, A., Broman, S.L., Hansen, A.S., Skov, A.B., Cacciarini, M., Kadziola, A., Kjaergaard, H.G., Mikkelsen, K.V., and Nielsen, M.B. (2016). Solar thermal energy storage in a photochromic macrocycle. Chemistry *22*, 10796–10800.

21. Edel, K., Yang, X., Ishibashi, J.S.A., Lamm, A.N., Maichle-Mössmer, C., Giustra, Z.X., Liu, S.Y., and Bettinger, H.F. (2018). The dewar isomer of 1,2-dihydro-1,2-azaborinines: isolation, fragmentation, and energy storage. Angew. Chem. Int. Ed. Engl. *57*, 5296–5300.

22. Kucharski, T.J., Ferralis, N., Kolpak, A.M., Zheng, J.O., Nocera, D.G., and Grossman, J.C. (2014). Templated assembly of photoswitches significantly increases the energy-storage capacity of solar thermal fuels. Nat. Chem. *6*, 441–447.

23. Masutani, K., Morikawa, M.A., and Kimizuka, N. (2014). A liquid azobenzene derivative as a solvent-free solar thermal fuel. Chem. Commun. (Camb.) *50*, 15803–15806.

24. Han, G.G.D., Li, H., and Grossman, J.C. (2017). Optically-controlled long-term storage and release of thermal energy in phase-change materials. Nat. Commun. *8*, 1446.

25. Dreos, A., Börjesson, K., Wang, Z., Roffey, A., Norwood, Z., Kushnir, D., and Moth-Poulsen, K. (2017). Exploring the potential of a hybrid device combining solar water heating and molecular solar thermal energy storage. Energy Environ. Sci. *10*, 728–734.

26. Dreos, A., Wang, Z., Udmark, J., Ström, A., Erhart, P., Börjesson, K., Nielsen, M.B., and Moth-Poulsen, K. (2018). Liquid norbornadiene photoswitches for solar energy storage. Adv. Energy Mater. *8*, 1–9.

27. Mansø, M., Petersen, A.U., Wang, Z., Erhart, P., Nielsen, M.B., and Moth-Poulsen, K. (2018). Molecular solar thermal energy storage in photoswitch oligomers increases energy densities and storage times. Nat. Commun. *9*, 1945.

28. Wang, Z., Roffey, A., Losantos, R., Lennartson, A., Jevric, M., Petersen, A.U., Quant, M., Dreos, A., Wen, X., Sampedro, D., et al. (2018). Macroscopic heat release in a molecular solar thermal energy storage system. Energy Environ. Sci. *12*, 187–193.

29. Neumann, O., Urban, A.S., Day, J., Lal, S., Nordlander, P., and Halas, N.J. (2013). Solar vapor generation enabled by nanoparticles. ACS Nano *7*, 42–49.

30. Ghasemi, H., Ni, G., Marconnet, A.M., Loomis, J., Yerci, S., Miljkovic, N., and Chen, G. (2014). Solar steam generation by heat localization. Nat. Commun. *5*, 4449.

31. Ni, G., Li, G., Boriskina, S.V., Li, H., Yang, W., Zhang, T., and Chen, G. (2016). Steam generation under one sun enabled by a floating structure with thermal concentration. Nat. Energy *1*, 16126.

32. Tao, P., Ni, G., Song, C., Shang, W., Wu, J., Zhu, J., Chen, G., and Deng, T. (2018). Solar-driven interfacial evaporation. Nat. Energy *3*, 1031–1041.

33. Kashyap, V., Al-Bayati, A., Sajadi, S.M., Irajizad, P., Wang, S.H., and Ghasemi, H. (2017). A Flexible anti-clogging graphite film for scalable solar desalination by heat localization. J. Mater. Chem. A *5*, 15227–15234.

34. Kashyap, V., Medhi, R., Irajizad, P., Jafari, P., Nazari, M., Masoudi, A., Marquez, M.D., Lee, T.R., and Ghasemi, H. (2019). Capture and conversion of carbon dioxide by solar heat localization. Sustain. Energy Fuels *3*, 272–279.

35. Dongare, P.D., Alabastri, A., Pedersen, S., Zodrow, K.R., Hogan, N.J., Neumann, O., Wu, J., Wang, T., Deshmukh, A., Elimelech, M., et al. (2017). Nanophotonics-enabled solar membrane distillation for off-grid water purification. Proc. Natl. Acad. Sci. USA *114*, 6936–6941.

36. Li, X., Lin, R., Ni, G., Xu, N., Hu, X., Zhu, B., Lv, G., Li, J., Zhu, S., and Zhu, J. (2018). Three-dimensional artificial transpiration for efficient solar waste-water treatment. Natl. Sci. Rev. *5*, 70–77.

37. Yang, J., Pang, Y., Huang, W., Shaw, S.K., Schiffbauer, J., Pillers, M.A., Mu, X., Luo, S., Zhang, T., Huang, Y., et al. (2017). Functionalized graphene enables highly efficient solar thermal steam generation. ACS Nano *11*, 5510–5518.

38. Zhou, L., Tan, Y., Ji, D., Zhu, B., Zhang, P., Xu, J., Gan, Q., Yu, Z., and Zhu, J. (2016). Self-assembly of highly efficient, broadband plasmonic absorbers for solar steam generation. Sci. Adv. *2*, e1501227.

39. McEnaney, K., Weinstein, L., Kraemer, D., Ghasemi, H., and Chen, G. (2017). Aerogel-based solar thermal receivers. Nano Energy *40*, 180–186.

40. Coscia, K., Nelle, S., Elliott, T., Mohapatra, S., Oztekin, A., and Neti, S. (2013). Thermophysical properties of $LiNO_3$ –$NaNO_3$ –KNO_3 mixtures for use in concentrated solar power. J. Sol. Energy Eng. *135*, 034506.

41. Cabeza, L.F., Gutierrez, A., Barreneche, C., Ushak, S., Ángel, G., Fernádez, A.I., and Grágeda, M. (2015). The opportunities of lithium in thermal energy storage: a state-of-the- art review. Renew. Sustain. Energy Rev. *42*, 1106–1112.